Fish foot prints

Mueller, U.K; van den Heuvel, B.L.E.; Stamhuis, Eize; Videler, J.J

Published in:
Journal of Experimental Biology

Publication date:
1997

The Journal of Experimental Biology 200, 2893–2906 (1997)
Printed in Great Britain © The Company of Biologists Limited 1997
JEB0904

FISH FOOT PRINTS: MORPHOLOGY AND ENERGETICS OF THE WAKE BEHIND A CONTINUOUSLY SWIMMING MULLET (*CHELON LABROSUS* RISSO)

U. K. MÜLLER*, B. L. E. VAN DEN HEUVEL, E. J. STAMHUIS AND J. J. VIDELER
Department of Marine Biology, University of Groningen, The Netherlands

Accepted 18 August 1997

Summary

The structure of the wake behind a continuously swimming mullet was analysed qualitatively and quantitatively by applying two-dimensional particle image velocimetry. A detailed analysis of the flow pattern and of the swimming movements of the fish allowed us to derive a kinematic explanation of the flow pattern as well as an estimate of the relative contributions of the body and the tail to thrust production. During active propulsion, the undulatory swimming fish shed a wake consisting in the medio-frontal plane of a rearward, zigzagging jet flow between alternating vortices. The fish shed one vortex per half tailbeat when the tail reached its most lateral position. Part of the circulation shed in the vortices had been generated previously on the body by the transverse body wave travelling down the body. This undulatory pump mechanism accounted for less than half of the energy shed in the wake. The remainder was generated by the tail. The vortex spacing matched the tailbeat amplitude and the stride length.

Key words: swimming, locomotion, flow field, wake structure, particle image velocimetry, mullet, *Chelon labrosus*.

Introduction

A swimming fish produces thrust by adding momentum to the water. Many species accelerate water along their body with waves of lateral undulations running from head to tail. These undulating movements are initiated by alternating waves of contraction of muscles arranged in myotomes on the left and right sides of the body. The phase relationship between the waves of muscle activation and the actual wave of the body is determined by the timing and speed of the waves of muscle contraction and by the reactive forces from the water on the fish (Hess and Videler, 1984). The effect of the reactive forces depends largely on the shape of the body and the mechanical properties of the body and tail. During steady swimming, the interaction between fish and water varies among swimming modes of fish species with different body forms, following a consistent pattern with several distinguishable kinematic modes (Wardle *et al.* 1995). One of these is represented by fish such as saithe *Pollachius virens* and mackerel *Scomber scombrus*, in which, during steady swimming, the amplitude of the lateral movements increases sharply over the posterior third of the body. A combination of kinematic and dynamic analyses of steady swimming in these species suggests that thrust is generated in discrete pulses at the tail blade (Videler and Hess, 1984; Hess and Videler, 1984). Proof that this actually happens should come from quantitative flow visualisation.

Several attempts have been made to visualise the wakes of fish, and a variety of techniques have been employed. Gray (1968) and Hertel (1966) added small particles to the water to show the patterns caused by a continuously swimming eel (*Anguilla anguilla*) and a water snake (*Natrix natrix*). Both animals shed a wake consisting of two alternating rows of vortices with a zigzagging jet between them. The first experiments on saithe- and mackerel-type swimmers used streak flow visualisation. Rosen (1959) used milk to visualise the flow directly under a continuously swimming pearl danio *Brachydanio albolineatus*. McCutchen (1977) made use of the different diffraction indices of water layers with different temperatures to visualise the wake of a zebra danio *Brachydanio rerio*. Aleyev (1977) injected dye into the oral cavity of several fish species. The blue dye escaped through the gill clefts together with the expired water into the wake of the fish. Rosen (1959) found indications of a regular vortex pattern behind continuously swimming fish, as did Aleyev (1977). McCutchen (1977), studying unsteady swimming, did not observe such a wake pattern. The first quantitative measurements in the wake of an undulatory swimming trout *Oncorhynchus mykiss* were made by Blickhan *et al.* (1992) using two-dimensional particle image velocimetry (PIV). From two-dimensional recordings, they reconstructed a three-dimensional impression of the wake and found evidence for a chain of alternating, almost circular, vortex rings and a zigzagging, caudal jet flow through the rings. Independently,

*Present address: Department of Zoology, Cambridge University, Downing Street, Cambridge, CB2 3EJ, UK (e-mail: ukm20@cam.ac.uk).

Videler (1993) predicted a similar pattern on the basis of the available data and hydrodynamic principles: vertical standing vortices, left behind at the turning points of the tail strokes, are connected by the dorsal and ventral tail tip vortices to form vortex rings. Consecutive vortex rings share the vertical vortices to form a chain of vortices.

Particle image velocimetry (PIV) techniques were used to quantify the wake of flying birds (Spedding *et al.* 1984; Spedding, 1986, 1987). Spedding *et al.* (1984) developed a method with which to calculate thrust from the vortex structures shed by a bird. The formalism is applicable to any regular vortex ring structure conforming to the assumptions and geometrical restrictions of the model. The model assumes that all the energy shed by the flying or swimming animal is contained in circular vortex rings and uses the size and the circulation of the rings to assess thrust and waste energy. It derives these estimates from two-dimensional cross sections through the wake. The cross-sectional view through a vortex ring consists of two vortices of opposite rotational sense. Assumptions are made that the distance between two consecutive vortices is the diameter of the vortex ring and that the circulation in the cross-sectional plane of the vortex represents the circulation of the entire vortex ring.

We have developed a two-dimensional PIV system to visualise the flow generated by animal movements (Stamhuis and Videler, 1995). Applying these quantitative PIV techniques to undulatory swimmers will yield velocity vector fields in one plane as primary data sets. Derived data on divergence, vorticity and vortex circulation allow estimates of the costs of swimming from the momentum shed in the wake.

Materials and methods

Experimental animals

The experiments were performed on a thick-lipped mullet *Chelon labrosus* Risso. Mullet are planktivorous cruisers that swim by undulating their body. The juvenile mullet used in this study (age 2 years, body length 0.12 m) was bred in captivity and held in a 40 l tank containing artificial sea water (salinity 30 %) at 22±1 °C.

Flow visualisation

We used two-dimensional particle image velocimetry (PIV) to visualise the water movements induced by the swimming fish (Stamhuis and Videler, 1995). The water (salinity 30 ‰, temperature 22 °C) in the test aquarium (1.5 m×0.3 m×0.5 m) was seeded with unexpanded polystyrene particles (VF 654, BASF, diameter 0.2–0.4 mm). Polystyrene has a slightly higher density than water of 30 ‰ salinity at 22 °C. The sinking speed of the particles could be neglected because it was low compared with the flow velocities in the flow patterns studied. The difference in density caused a small time lag in the response of the particle to the fish-generated currents (Merzkirch, 1974); we ignored this effect. The particles were illuminated in a horizontal plane by a laser light sheet (krypton laser, beam 1 mm thick, wavelength 647 nm, maximum power 0.8 W).

Experiments were performed with one individual in the test aquarium and lasted 2 h. The fish was placed into the test aquarium 1 day prior to the experiments. We did not train or stimulate the fish in any way. All swimming behaviour observed was spontaneous. The fish cruised up and down in the middle of the aquarium. When passing the light sheet, the fish kept its eyes above or below the light level, but otherwise seemed undisturbed in its swimming behaviour. Recordings were made when the fish was swimming in the field of view of the camera. Immediately prior to the experiments, we reduced the water level to a depth of 10 cm to increase the chance of the fish swimming through the light sheet. In the field of view, the water surface was covered with a Perspex raft to avoid surface waves distorting the image.

The camera (CCD camera: Adimec MX-12, 50 mm lens) was mounted to record top-view images of 512×512 pixels at a frequency of 25 images s^{-1}. With a field of view of 195 mm×195 mm, this yields a spatial resolution of 1 pixel representing a space of 0.4 mm×0.4 mm. The gain of the camera was set to achieve maximal contrast between the lit-up particles and a dark background. The shutter opened for only 8 ms for each frame to avoid motion blur of the particles. Recorded images were digitised in real time and stored uncompressed on computer hard disk. Sequences used for further analysis were selected from the stored raw data. Here, we report on sequences in which the fish swam in the light sheet at a constant speed along a straight path.

Kinematic analysis

We programmed applications within an image-analysis environment (TIM, DIFA measuring systems) to obtain the midline and several kinematic parameters of the fish. The contour of the fish in each image was digitised manually. The closed contour was filled and then eroded to obtain the midline. The positions of the head and the tail tip had to be indicated manually to anchor the erosion and avoid artificial shrinking of the fish. This procedure yielded a description of the midline consisting of up to 300 x,y-coordinate pairs.

The body length L of the fish was assumed to be equivalent to the number of pixels representing the midline. The head coordinates in subsequent pictures were used to calculate the mean path of motion and the instantaneous swimming speed. The mean path of motion was calculated over complete tailbeat cycles using standard linear regression. The instantaneous swimming speed U was calculated from the displacement of the head between frames. If the mean value of U over one complete tailbeat cycle did not change significantly from one cycle to the next, the fish was assumed to be swimming at a constant speed.

All pixel coordinates of the midline were transformed so that the mean path of motion ran along the x-axis. The midline was smoothed using a weighted 11-point running average to remove the high-frequency noise caused by the pixel nature of

the midline coordinates. We also calculated the position of the inflection points on the midline. These are points where the curvature of the midline changes from concave to convex or *vice versa*. Inflection points were calculated numerically by finding the extremes in the slope of the smoothed midline for consecutive pixels.

The kinematics of an undulatory swimmer can be described in terms of a body wave and a propulsive wave (Gray, 1933). The fish body shows a lateral wave in a fish-related frame of reference with a posteriorly increasing amplitude A_b and a wave length λ_b travelling along the body in the caudal direction at a speed V. Every point on the body describes a wave in an earth-bound frame of reference with an amplitude A_s and a wavelength λ_s travelling forward at a speed U identical to the mean swimming speed of the fish.

The wavelength λ_b of the body wave was calculated as twice the distance between the zero crossings of the body wave, i.e. the points where one particular midline crosses the path of motion. The amplitude A_b of the body wave was calculated from the unsmoothed midlines as half the transverse distance between the points of maximum lateral excursion of a particular body segment. The wave speed V along the body was calculated from the displacement of the zero crossing along the body midline. The length λ_s, the amplitude A_s and the phase p_b of the propulsive wave were calculated from the x and y displacements of the wave crest in an earth-bound frame of reference. The length λ_s of the propulsive wave was calculated as twice the distance between zero crossings of a particular point on the midline. The amplitude A_s of a particular body segment is identical to the body wave amplitude A_b at this particular segment along the body.

Hydrodynamic analysis

Data processing

Particle image velocimetry (PIV). Flow velocity vectors were obtained by conducting a subimage cross-correlation on two successive images (Chen *et al.* 1993; Stamhuis and Videler, 1995). The cross-correlation routine finds the most probable average particle displacement in a particular region of the flow by calculating the correlation between two subimages from the same location in two consecutive frames. We used a subimage size of 39 pixels × 39 pixels to ensure a minimum seeding of 10 particles per subimage (Keane and Adrian, 1991). With consecutive subimages overlapping by 50 % for maximum spatial resolution without over-interpreting the data (Hinsch, 1993), this yielded a vector field of, at best, 26×26 equally spaced vectors, if all subimages contained sufficient information for cross-correlation.

Particle tracking velocimetry (PTV). The correlation routine only calculates reliable velocity vectors for subimages with at least 10 particles, a mean particle displacement of less than 25 % of the subimage diameter and a mainly translational flow component (Keane and Adrian, 1991). Areas with a low seeding, strong rotational flow or high flow velocities had to be analysed by marking corresponding particle pairs manually. This applied in particular to the wake immediately after shedding. The position and the magnitude of the velocity vectors were obtained from the centres of mass of each indicated particle pair (Stamhuis and Videler, 1995). This yielded a subpixel spatial resolution for the PTV velocity vector field. Comparing PTV and PIV data shows that the averaging process internal to the cross-correlation routine does not greatly affect the value of the maximum flow velocities: the maximum displacement of a particle between two consecutive frames as measured from the original recordings by PTV was 16 pixels or 6.0 mm. The flow field resulting from PIV showed a maximum displacement of 5.7 mm, an underestimation of the peak flow velocity of 5 %. The mean displacement of a particle was 2.8±2.6 pixels or 1.1±1.0 mm (mean ± S.D., N=982) between consecutive frames.

Post-processing. The original flow velocity vectors were fitted into a user-defined grid of either 26 cells × 26 cells (vector fields based on PIV) or 40 cells × 40 cells (vector fields resulting from a combination of PIV and PTV data). All vectors in one grid cell were averaged, the resulting vector was evaluated using an error routine, and a two-dimensional spline routine interpolated vectors to fill gaps in the vector field (Stamhuis and Videler, 1995). From the flow velocity vector field, we derived the following flow parameters: vorticity ω describing the angular velocity in the fluid; divergence θ, a parameter that in a two-dimensional flow field gives an indication of the out-of-plane movement of the water; and the discriminant for complex eigenvalues d, which was used to locate the centre of vortices (Stamhuis and Videler, 1995).

Wake morphology parameters were calculated from PIV data after post-processing: the distance between vortices along and perpendicular to the path of motion as well as the momentum angle φ (Fig. 1) of a vortex pair were calculated from the position of the vortex centres in the flow field; the angle α between the jet flow and the path of motion was obtained as a mean value from the angles of the velocity vectors in the jet. All mean values in the text are given with standard deviations (S.D.).

Five image pairs were analysed by the more labour-intensive PTV method to obtain a more detailed picture of the flow field in the vicinity of the fish's body and of the velocity distribution within the vortices. Vortex parameters were derived from the original PTV data to retain the high spatial resolution of the original PTV data set. We calculated the flow velocity component u parallel to the line x' connecting two adjacent vortices and the flow velocity component v perpendicular to the line y' connecting two adjacent vortex centres (Fig. 1). The profiles were described by the radii of the vortex cores and of the vortex rings. The core radius R_0 was calculated as half the distance between the extremes in the velocity profile of the velocity component u (Fig. 2A). The ring radius R between two adjacent vortices was calculated as half the distance between the outer extremes in the v velocity profile minus the core

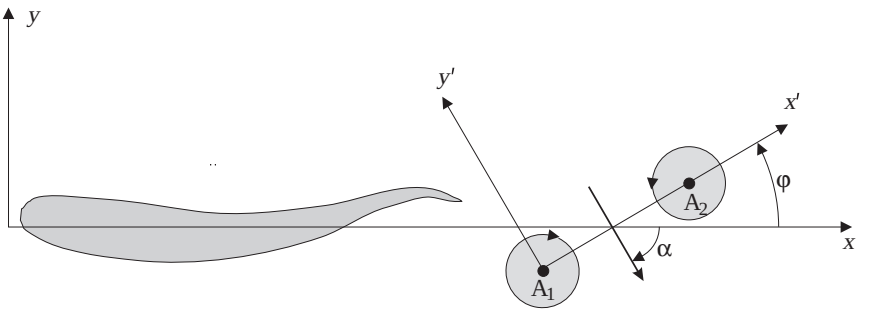

Fig. 1. Coordinate system and notation used to describe swimming kinematics and the wake. The original image coordinates were transformed so that the fish swam along the *x*-axis and the lateral body undulations are in the direction of the *y*-axis. The fish shed the vortices A_1 and A_2, which as a vortex system were inclined by a momentum angle φ relative to the mean path of motion *x*. The vortices A_1 and A_2 are separated by a jet flow (bold arrow) crossing the mean path of motion *x* at an angle α. The velocity distribution within the vortex is represented within a coordinate system with the *x*′-axis running through the centres of two adjacent vortices and the *y*′-axis perpendicular to *x*′.

radius R_0 (Fig. 2B). The vorticity ω (Fig. 2C) was obtained from the PTV velocity vector field according to:

$$\omega = \frac{\partial v}{\partial x'} - \frac{\partial u}{\partial y'}. \quad (1)$$

Energy calculations

We calculated thrust and waste power from the wake using a vortex chain model, originally developed for bird flight (Rayner, 1979; Spedding *et al.* 1984). We assumed the vortices to be circular and to contain all vorticity. The circulation Γ of the vortex was calculated according to Spedding *et al.* (1984), with *C* being a closed curve around the vortex centre:

$$\Gamma = \oint_C v\,dy'. \quad (2)$$

The flow phenomena visible in the medio-frontal plane of the fish are the start–stop vortices. Each of these can be interpreted as part of the vertical component of two vortex rings linked in a chain. We therefore assume that the circulation measured in the medio-frontal plane is equivalent to the added circulation of two rings. We obtain the vortex ring momentum *I* of a single vortex ring using half the measured circulation according to:

$$I = \rho_w \tfrac{1}{2}\Gamma\pi R^2, \quad (3)$$

leading to the thrust energy E_T gained by shedding one vortex ring:

$$E_T = \tfrac{1}{2} I U \sin\varphi, \quad (4)$$

and the self-energy of the vortex E_L:

$$E_L = 0.5\rho_w \Gamma^2 R[\ln(8R/R_0) + B - 2]. \quad (5)$$

B is a constant depending on the vorticity across the vortex core. Here, we followed Spedding *et al.* (1984) and used a value of 0.25.

Results

One sequence lasting 5 s was selected from 90 h of recording that satisfied the following criteria: the fish was swimming

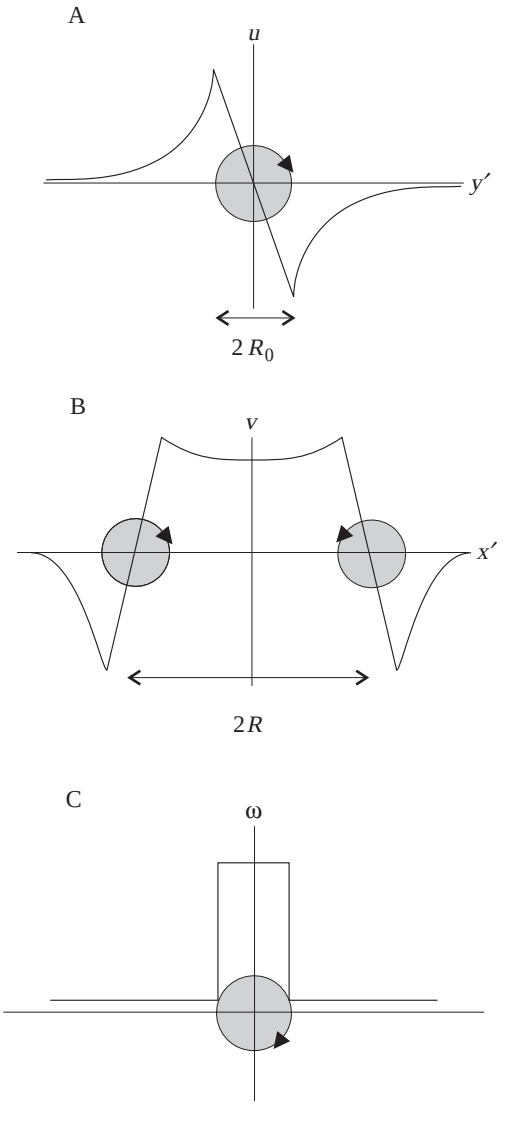

Fig. 2. Profiles of a Rankine vortex ring (after Spedding, 1987). The shaded circles and arrowheads indicate the size and rotational sense of the vortex core. All profiles are taken through the centre of the vortex cores. (A) Distribution of the flow velocity component *u* along the *y*′-axis; the vortex core diameter $2R_0$ is indicated. (B) Distribution of the flow velocity component *v* along the *x*′-axis; the vortex ring diameter 2*R* is indicated. (C) Distribution of vorticity ω along the radius of the vortex ring for an ideal fluid.

Table 1. *Mean morphological and kinematic parameters for one sequence of straight swimming at constant speed by* Chelon labrosus

Parameter	Units	Mean	S.D.	*N*
Body length *L*	m	0.126	0.006	7
Swimming speed *U*	$m\,s^{-1}$	0.175	0.041	27
	$L\,s^{-1}$	1.4	0.3	
Maximum angle of attack	degrees	31		
Tailbeat frequency *f*	s^{-1}	3.86	0.24	4
Tailbeat amplitude A_{tail}	*L*	0.09	0.01	5
Stride length λ_s	*L*	0.53	0.05	17
Body wavelength λ_b	*L*	1.11	0.02	7
Slip *U*/*V*		0.7	0.1	8
Strouhal number *St*		0.34		

V, propulsive wave speed.

horizontally in the light sheet at a constant swimming speed in a straight line shedding a wake within full view of the camera (Table 1). Forty image pairs were analysed fully, ranging from the moment when the fish entered the field of view to 1 s after the fish left the camera range.

Swimming kinematics

The fish swam continuously from the lower right to the upper left of the image at a speed *U* of $0.175\pm0.041\,m\,s^{-1}$ ($1.4\pm0.3\,L\,s^{-1}$) (*N*=27) using 2.5 tailbeats to complete the crossing. The swimming speed varied during the tailbeat cycle between $0.160\,m\,s^{-1}$ when the tail has crossed the mean path of motion and was approaching a lateral extreme position and $0.220\,m\,s^{-1}$ when the tail had passed the lateral extreme position and was approaching the mean path of motion. The swimming kinematics is characterised by the body wave of wavelength λ_b and the propulsive wave of wavelength λ_s. The amplitude of the body wave decreased from the head to the pivot point at 0.3*L* and then increased curvilinearly from the pivot point to the tail (Fig. 3A). The tailbeat amplitude was 0.011 ± 0.001 m ($0.09\pm0.01L$) (*N*=5). The phase p_b of the body wave increased linearly from head to tail (Fig. 3B). This agrees with the typical body wave of a saithe- or mackerel-type swimmer (Wardle *et al.* 1995). The body wavelength was $1.11\pm0.02L$ (*N*=7). The propulsive wavelength was $0.53\pm0.05L$ (*N*=17). The ratio of the swimming speed *U* to the propulsive wave speed *V* was 0.7 ± 0.1 (*N*=8), indicating that the fish was producing thrust (Gray, 1933). The duration of one tailbeat cycle *T* was 0.26 ± 0.016 s (*N*=4). The angle of the tail with respect to the path of motion varied between 0 ° when the tail was at its most lateral position to 49 ° when the tail was crossing the path of motion (*T*=0). The lateral velocity of the tail tip varied out of phase with the swimming speed *U* between $0\,m\,s^{-1}$ when the tail was in its most lateral position and $0.26\pm0.06\,m\,s^{-1}$ (*N*=5) when the tail was approaching the mean path of motion.

Flow field in the vicinity of the fish

Fig. 4 shows the flow in the vicinity of the fish's body. Only particle displacements in the *xy* plane at the level of the medio-

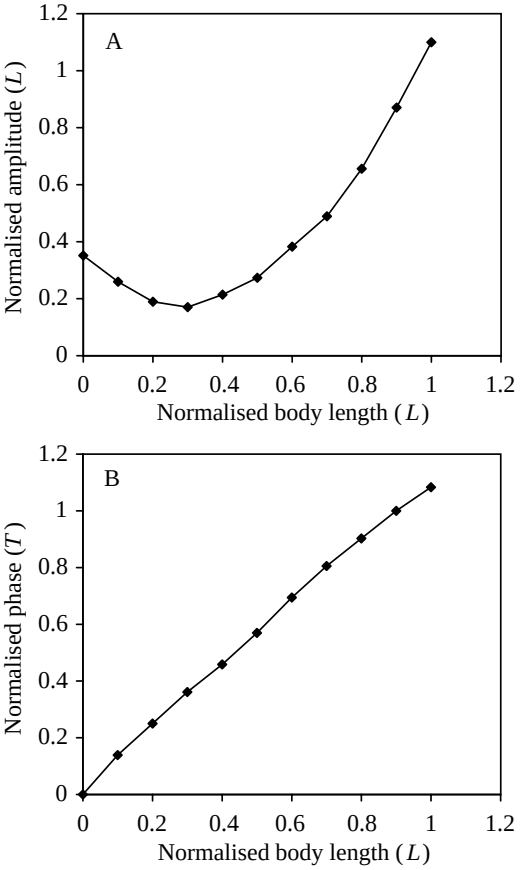

Fig. 3. Amplitude and phase of the body wave of a steadily swimming mullet. The unit of time is the duration *T* of the tailbeat. The instant when the tail crosses the path of motion was arbitrarily chosen to be at *T*=0. (A) Lateral deflection along the fish's body. (B) Phase of the maximum lateral deflection as a function of the position along the fish's body.

frontal plane of the fish are visible. The fish casts a shadow to its left, obscuring the flow pattern in the bottom part of the flow field.

Near the head, the water is pushed away and accelerated. In our two-dimensional images of the *xy* plane, the water displacement in the *z*-direction can be traced by calculating the divergence of the flow (Stamhuis and Videler, 1995). This parameter peaks in front of the head, indicating that the water is thrust to the side as well as upwards and downwards. The peak in the flow speed due to this effect of the head is $18\pm4\,mm\,s^{-1}$ (*N*=14), averaged over two tailbeat cycles. Fig. 4 also shows a stagnation point in the flow directly in front of the head.

The body undulations cause local speed maxima in the flow adjacent to the fish's body (Fig. 4). As the undulatory wave passes down the body, the pressure and suction flows travel caudally along with the concave and convex bends. The peak speeds adjacent to the maximal lateral excursion of the fish's body increase along the body from $20\,mm\,s^{-1}$ at 0.2*L* to $50\,mm\,s^{-1}$ or more when the wave crest reaches the peduncle. In the tail region, the pressure and suction flows combine with

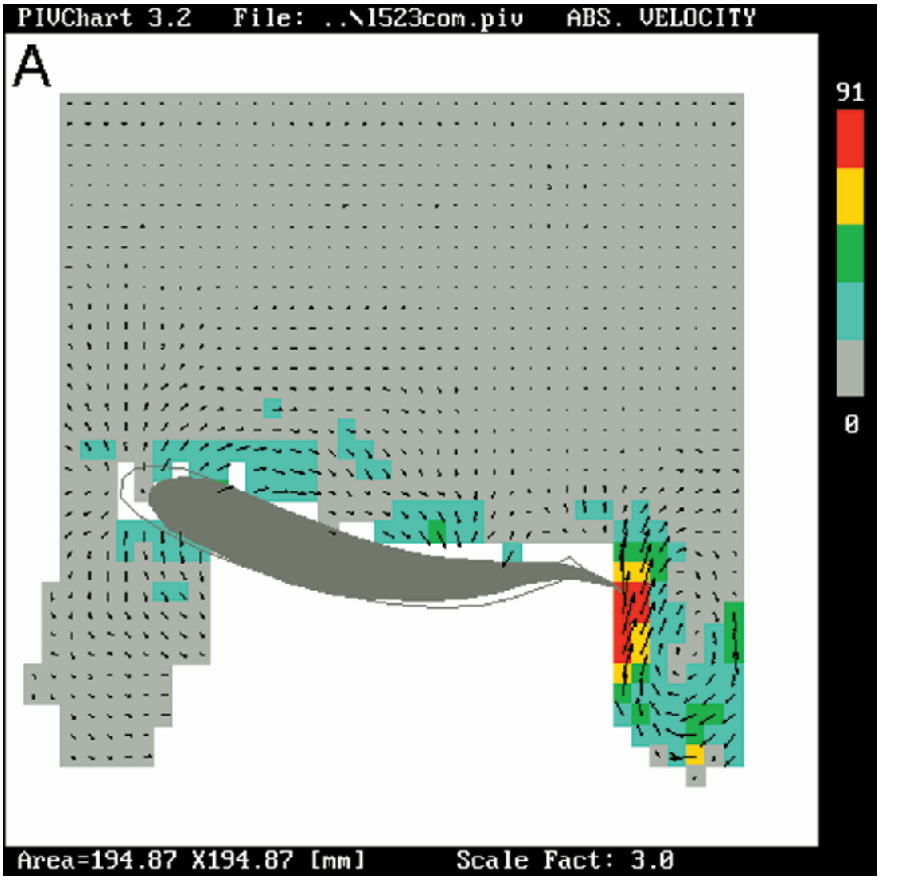

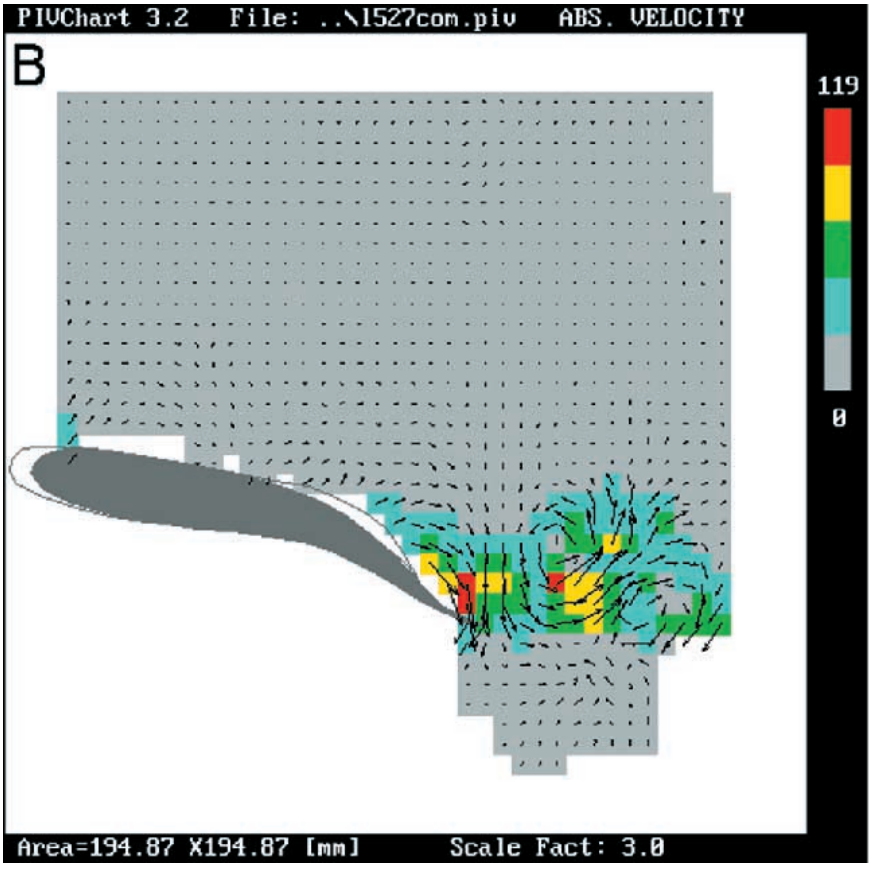

Fig. 4. Flow velocities in the vicinity of the fish when the tail has reached a lateral extreme position (field of view 0.195 m×0.175 m). The vector information was obtained by combining PIV and PTV data. The colour code indicates the magnitude of the flow velocity; the arrows represent the flow velocity in mm s^{-1}. (A) Velocity vector field on the concave side of the fish's body as the tail reaches a lateral extreme position to the right. (B) Velocity vector field on the convex side of the body as the tail reaches a lateral extreme position to the left. (C) Velocity vector field on the concave side of the fish's body as the tail approaches the mean path of motion. The flow field in C is based on PIV data alone.

the circulatory flow around the tail into a vortex that is shed when it is at its most lateral position. Peak flow speeds of up to 100 mm s^{-1} occur at the tail when the tail is crossing the mean path of motion (Fig. 4C). Peak flow speeds are at a minimum of approximately 50 mm s^{-1} when the tail is at its most lateral position and is changing direction. Averaged over two tailbeat cycles, the peak flow at the tail has a speed of 74±34 mm s^{-1} (N=34) and points away from the fish at an angle of 44±14° (N=34) to the mean path of motion.

Flow in the wake of the fish

Wake morphology

Fig. 5 shows the flow in the xy plane as the fish leaves the field of view (Fig. 5). When the tail reaches its maximum lateral excursion and changes direction, a vortex is shed at the tail tip. Vortices shed to the left-hand side of the animal rotate clockwise, vortices shed to the right-hand side rotate counter-clockwise. The distance l_y between two consecutive vortices in the y direction is 0.18±0.07L (N=47), this distance l_x in the x direction is 0.26±0.09L (N=49) (Table 2).

Between two consecutive vortices, a jet flow is visible pointing obliquely sideways and away from the fish. The jet changes direction with every new vortex being shed, giving the jet flow an undulating shape. The angle α between the direction of the jet flow and the mean path of motion is 44.5±7.5° (N=61).

Vortex morphology

The velocity and vorticity profiles of the vortices in the wake (Fig. 6) resemble the main characteristcs of a Rankine-type vortex (Fig. 2). A Rankine vortex is a hypothetical structure. It has a core in solid-body rotation with zero velocity at the centre and the velocity increasing linearly towards the edge of the vortex core; the core entrains the surrounding fluid to a potential flow region, with the flow velocity decreasing in inverse proportion to the distance from the core. The vorticity in the core is non-zero and constant; the vorticity in the potential flow is zero. The u/y' profiles of the vortices in the wake show two sharp velocity extremes close to the centre of the vortex marking the outer rim of the vortex core (Fig. 6A). Beyond these extremes, the flow velocity decreases curvilinearly, indicating the potential flow region. The vorticity profile of a vortex in a real fluid has no sharp transition from a finite constant vorticity value in the core to zero vorticity in the potential flow region, but viscous effects induce a more S-shaped profile (Maxworthy, 1977). In all image pairs analysed, the maxima in the vorticity vector fields coincide with the minima of d or are situated in a grid cell adjacent to the grid cell with the minima of d, supporting the evidence from the ω/R graph (Fig. 6C) that the vorticity is centred in the vortex core.

Over a period of 0.6 s after shedding, the vortex ring radius R stays constant (Table 3). The core at the moment of shedding

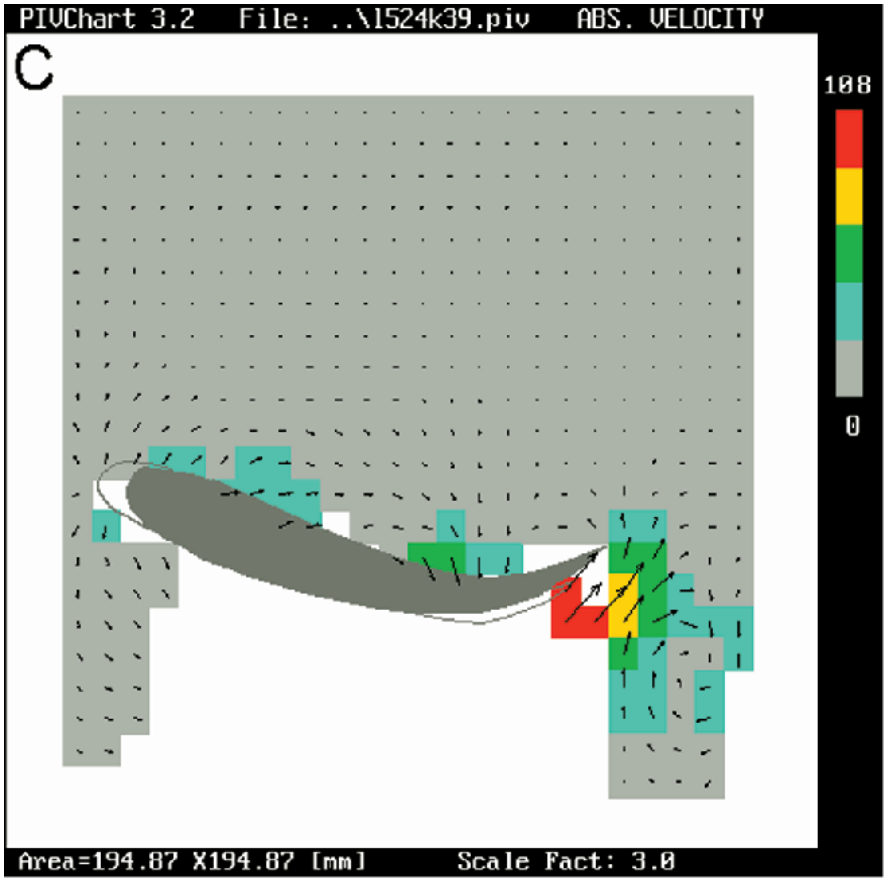

Table 2. *Wake morphology parameters obtained from the flow fields after post-processing, averaged over 0.6 s*

Wake parameter	Units	Mean	S.D.	*N*
Apparent ring radius R	m	0.019	0.004	16
Vortex spacing in y direction, l_y	L	0.18	0.07	47
Vortex spacing in x direction, l_x	L	0.26	0.09	49
Ring momentum angle φ	degrees	40	10	55
Jet angle α	degrees	44.5	7.5	61
Jet velocity	m s^{-1}	0.091	0.032	16
Core velocity	m s^{-1}	0.067	0.016	16

has a radius R_0 of 6–8 mm. After 0.6 s, the core radius R_0 has doubled. The peak flow velocity in the jet is 0.091±0.032 m s^{-1} (N=16) (Table 2); it does not decrease significantly over the 0.6 s time interval considered. The peak velocity at the rim of the vortex core reaches values of 0.067±0.016 m s^{-1} (N=16). This gives the vortex core a rotation frequency of 1.0±0.5 Hz (N=16).

Energy in the wake

Since the fish sheds two vortex rings per tailbeat cycle, we obtained thrust power P_T from thrust energy E_T and tailbeat frequency f according to:

$$P_T = E_T 2f. \quad (6)$$

For a fish swimming continuously at 1.4 L s^{-1}, we obtained a vortex circulation of 7.6×10^{-4} m^2 s^{-1}, resulting in a thrust energy of 0.07 mJ and a thrust power of 0.56 mW (Table 4), a vortex power of 0.02 mW and a hydrodynamic efficiency of 97 % for a vortex approximately 0.1 s after being shed. Over a period of 0.6 s, the thrust energy and thrust power calculated for one particular vortex decreased to 0.01 mJ and 0.1 mW, respectively. The precision of the energy calculation is limited by the grid resolution of the velocity vector field (Table 4).

Discussion

Linking kinematics and hydrodynamics

Several hypotheses have been put forward regarding the generation of a chain of vortex rings. Rosen (1959) and Blickhan *et al.* (1992) suggested mechanisms that hold the body responsible for a considerable part of wake generation. Lighthill (1969), Ahlborn *et al.* (1991) and Videler (1993) described a mechanism in which the vortex wake is generated exclusively by the tail.

Wake generation and body kinematics

Rosen (1959) suggested that the vortices he observed in his two-dimensional horizontal impressions of the wake were a result of the separation effects of a rolling-up boundary layer along the fish's body. We did not observe the attached vortices on the body described by Rosen (1959). Our flow fields support the concept of circulation generated on the body by the undulatory pump mechanism and of bound vortices at the tail, both types combining into a single free vortex upon being shed at the tail.

The undulating pump mechanism generating the vortex wake was first proposed by Blickhan *et al.* (1992): the alternating suction and pressure flows form a circulating flow around the inflection points of the body; this circulating flow is shed when the inflection point reaches the tail. Our results on the body kinematics together with the development of the flow patterns around a swimming mullet support this hypothesis. In Fig. 7A, the superimposed body contours show that the head contributes most significantly to the initial outward lateral water displacement. The contours on the convex side barely exceed the head contours, even in the tail region where the lateral displacement of the body reaches its maximum. The lateral movement of the body adds very little to the water volume displaced laterally. The largest lateral water displacements due to the body occur on the concave side where the body contour recedes considerably compared with the head contour (Fig. 7B). This receding movement generates strong suction flows towards the body of the fish. The flow velocities increase slowly along the first two-thirds of the body. The peak flow velocities on the concave side of the body do not exceed the velocities on the convex side for the first two-thirds of the body; peak values in the fluid adjacent to the body are between 0.02 and 0.03 m s^{-1}. In the last third of the body, where the body wave amplitude increases considerably, the peak velocities in suction zones reach values of up to 0.10 m s^{-1} in the tail region, whereas the peak velocities on the pressure side remain as low as 0.03 m s^{-1}. The lateral movements of the body create strong suction and weaker pressure flows in the posterior third of the body.

These maxima in the flow velocity at the points of maximum lateral excursion alternate with flow velocity minima at the

Table 3. *Vortex parameters obtained directly from the PTV data, averaged over 0.24 s*

Parameter	Units	Mean	S.D.	*N*
Ring radius R	m	0.019	0.004	16
Core radius R_0	m	0.012	0.004	16
Core radius/ring radius R/R_0		0.69	0.34	16

Table 4. *Energy calculations based on the wake momentum and the fish kinematic data*

Parameter	Units	Hydro* dynamics	Grid cell† precision	Kine-matics
Circulation Γ	m^2 s^{-1}	7.6×10^{-4}	1×10^{-5}	
Thrust energy E_T	mJ	0.073	0.004	
Vortex energy E_L	mJ	0.002	4×10^{-4}	
Efficiency η		0.971	0.001	0.586
Thrust power P_T	mW	0.563	0.016	0.185
Vortex power P_L	mW	0.017	0.001	0.131

*The hydrodynamic estimate is based on the flow field of a vortex ring shed 0.08 s ago. We used the mean value of the vortex ring diameter in the x' and y' directions to obtain the wake momentum.

†The grid cell precision gives the maximum error of the value due to the finite size of the grid and the averaging procedure of the post-processing.

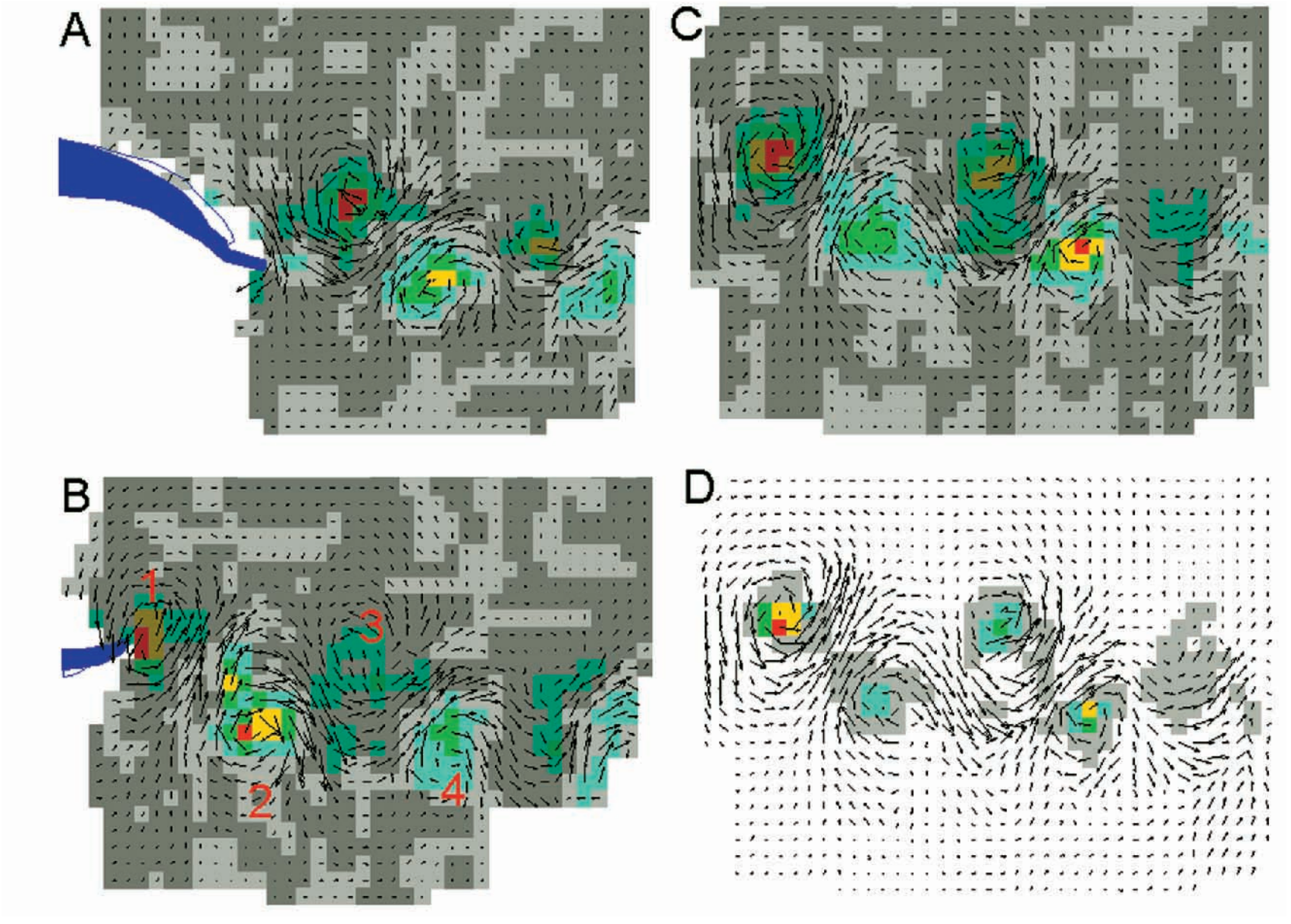

Fig. 5. The wake of a continuously swimming mullet (field of view 0.195 m×0.175 m); vector information was obtained by combining PIV and PTV data. The arrows represent the flow velocity in mm s^{-1}; the colour code represents vorticity in A–C, with bright shades indicating clockwise vorticity and dark shades indicating counter-clockwise vorticity; the colour code represents the discriminant for complex eigenvalues in D. (A) Vorticity ω at time 0 s. (B) Vorticity ω at time 0.16 s. The vortices are numbered from just shed (1) to older (2–4) vortices. (C) Vorticity ω at time 0.32 s. (D) Discriminant for complex eigenvalues *d* at time 0.32 s; *d* is at its most negative (red) in the centre of the vortices.

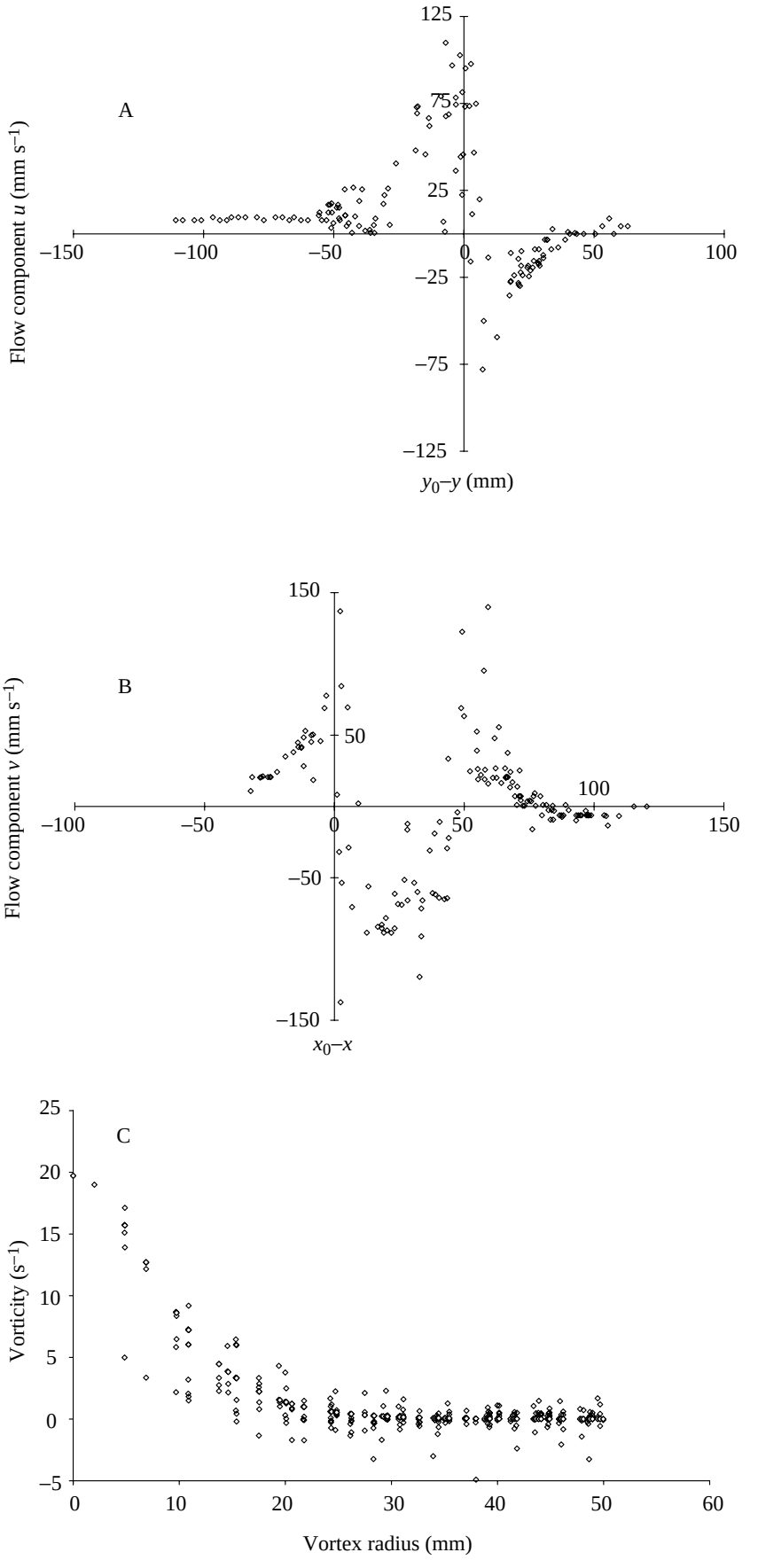

Fig. 6. Velocity and vorticity profiles of vortices from Fig. 5B. The transect runs through the core of the vortex; the width of the transect is 10 % of the vortex ring diameter. (A) u velocity profiles through vortex 1 from Fig. 5B. (B) v velocity profile through the vortex system formed by vortices 1 and 2 from Fig. 5B. (C) Vorticity ω profile of vortex 1 from Fig. 5B.

transition between suction and pressure zones. This transition coincides with a small peak in vorticity and occurs near two characteristic points of the body wave. One is the inflection point of the body wave, and the other is the crossing point between two consecutive midlines (Fig. 7C). The close vicinity of those two points constitutes the heart of the undulatory pump: the body appears to rotate around a point in space and to entrain the surrounding fluid to follow its rotating movement. The rotation centre travels down the body with a speed similar to the speed V of the body wave: both inflection point and crossing point travel backwards ($0.6\pm0.8V$, N=36, and $0.8\pm1.0V$, N=30, respectively) and away from the mean path of motion ($0.1\pm0.3V$, N=36, and $0.1\pm0.2V$, N=30, respectively) in an earth-bound frame of reference at speeds not significantly different from the propulsive wave speed V. As the inflection and the crossing point – along with the suction and pressure zones – travel down the body, the flow velocities in the suction and pressure zones increase.

Wake morphology versus *kinematic tail parameters: maximising efficiency of thrust production*

The hypotheses of Lighthill (1969), Ahlborn *et al.* (1991) and Videler (1993) interpret the vortex wake as a result of the tail kinematics. A bound vortex is built up around the tail as it sweeps from one side to the other during one tailbeat. As the tail changes direction when it reaches its most lateral displacement, this circulating flow is shed as a start–stop vortex and a new bound vortex is generated. Since there is one tip vortex at the upper tip and another tip vortex at the lower tip of the tail, two consecutive start–stop vortices form a vortex ring.

The wake of a continuously swimming mullet exhibits a flow pattern that is consistent with the assumption of such a three-dimensional vortex chain. In our two-dimensional view of the wake, only sections through the vertical ring component, i.e. start–stop vortices, are visible together with transects through the jet flow. We can thus support the evidence presented by Rosen (1959), Hertel (1966), Gray (1968), Aleyev (1977) and Blickhan *et al.* (1992) that such a vortex chain is characteristic of the wake behind a cruising undulatory swimmer.

The hypothesis of the tail-induced wake predicts some correspondence between tailbeat cycle, tail shape and wake morphology. In the continuously swimming mullet, the centres

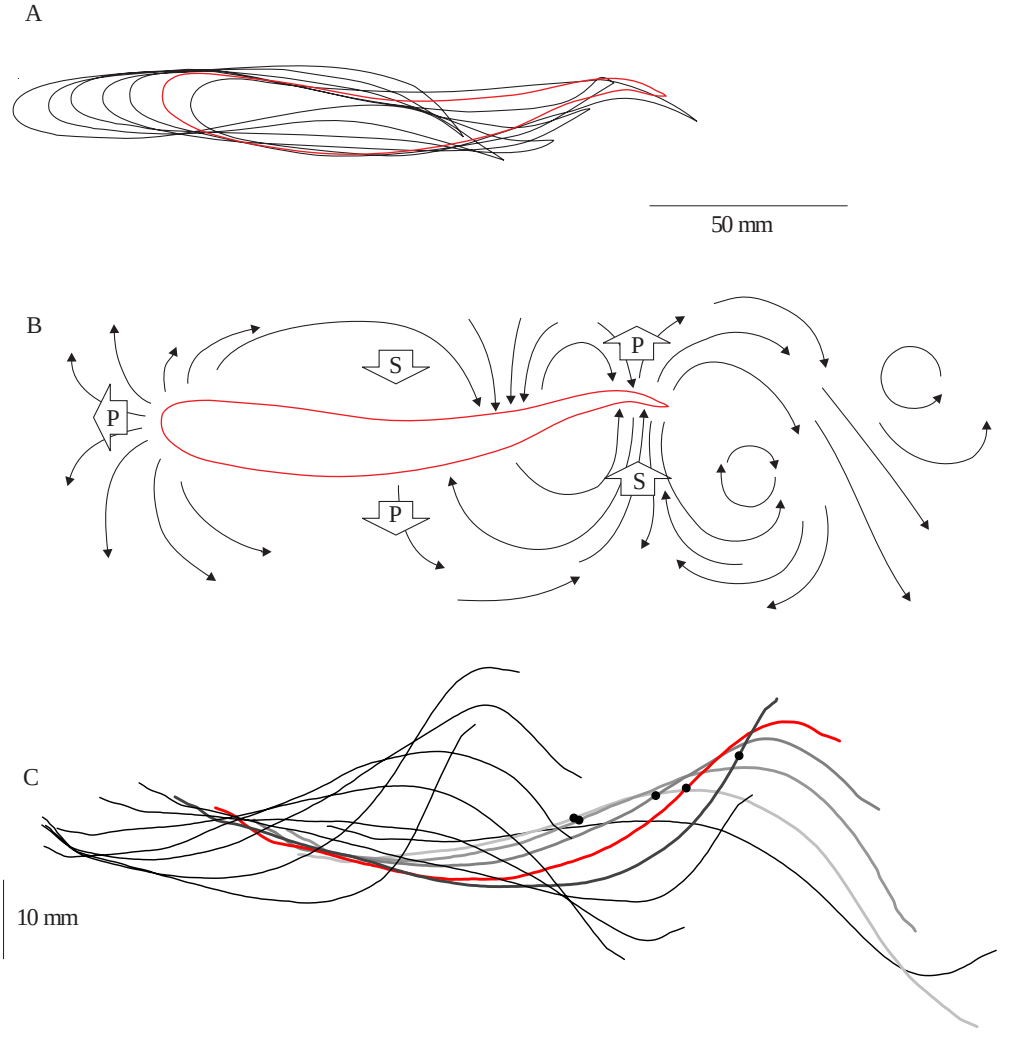

Fig. 7. Linking kinematics and hydrodynamics in a continuously swimming mullet. The contour and the midline of the fish shown in Fig. 4A are indicated in red. The horizontal scale applies to all parts of the figure. (A) Superimposed body contours of a swimming mullet for 1.5 tailbeat cycles. (B) Schematic drawing of the flow pattern in the vicinity of a swimming mullet. S, a suction zone adjacent to a concave bend in the body; P, a pressure zone adjacent to a convex bend in the body; arrows indicate the main flow directions. (C) Midlines of a swimming mullet for one tailbeat cycle. The circles on the midlines indicate inflection points. The vertical scale is enlarged with respect to the horizontal scale to emphasise the movements of the inflection point and the body wave.

of the vortices corresponded approximately to the position of the tail tip at the time of vortex shedding. The distance between the consecutive vortices in the direction of the mean path of motion (l_x=0.26±0.09L) was equivalent to half the stride length (0.53L) for vortices up to 0.6 s after being shed (Table 2). The distance between consecutive vortices perpendicular to the path of motion (l_y=0.18±0.07L) was twice the tailbeat amplitude (0.09L). We could detect no displacement of the shed vortices. After 1 s, the wake had deteriorated sufficiently to make the detection of most vortex centres impossible. The vortex ring diameter 2R in the xy plane (2×0.019 m) is twice the tail fin height (0.02 m). This would translate to an oval vortex ring, unlike the circular vortex rings described by Blickhan *et al.* (1992).

Lighthill (1969, 1970) showed theoretically that, for significant positive thrust production at high efficiency, the fish needs to tune its kinematics appropriately. Lighthill (1969, 1970) varied mainly the feathering parameter to find the optimal kinematics for good efficiency. The feathering parameter F expresses the orientation of the tail in the flow: it relates the angle between the tail fin and the mean path of motion to the angle of the tail path. F is the product of the stride length λ_s and the maximum angle β of the tail fin divided by twice the tailbeat amplitude A_{tail}:

$$F = \lambda_s\beta/2A_{tail}\,. \quad (7)$$

Lighthill (1969, 1970) concluded that feathering parameters between 0.6 and 0.8 are best for maintaining high efficiency. Triantafyllou *et al.* (1993) used the kinematic values suggested by Lighthill (1969, 1970) for optimum efficiency to conduct experiments on the efficiency of thrust production by a flapping foil. They used the Strouhal number St (the ratio of unsteady to inertial forces, a parameter used to describe oscillating phenomena in fluids) to describe the wake of the foil. The Strouhal number St is calculated according to:

$$St = (\text{frequency of vortex shedding} \times \text{width of the wake})/U\,. \quad (8)$$

Triantafyllou *et al.* (1993) found maximum efficiency for Strouhal numbers in the range 0.25–0.35.

The feathering parameter derived for mullet in the analysed swimming sequence was 0.7, which is within the optimum range; the Strouhal number was 0.34, also within the optimum range (Table 1). Triantafyllou *et al.* (1991, 1993) list a range of Strouhal numbers derived from the kinematic parameters of several fish species on the assumptions that the frequency of vortex shedding is twice the tailbeat frequency and that the width of the wake is twice the tailbeat amplitude. Our data show that this is a valid first approximation of the Strouhal number. The values of these estimates in the present study are close to the optimum range for all fish species considered.

Fish seem to tune their kinematics to produce an optimal wake for maximal hydrodynamic efficiency. Using Spedding's (Spedding *et al.* 1984) calculation method for hydrodynamic efficiency, we calculate a value of greater than 90 % for an actively swimming mullet at a Strouhal number of 0.34.

Swimming energetics: various methods to estimate costs

The external costs of swimming can be estimated using two approaches. The hydrodynamic approach measures flow parameters and deduces the costs of swimming from the size and the flow velocities of the wake. The kinematic approach uses the kinematic parameters describing the swimming movements of the fish and estimates the swimming energetics, inferring the flow and its energetic consequences from the fish's movements. One possible hydrodynamic approach is based on estimating the energy shed in the form of vortex rings (Spedding *et al.* 1984). The backward momentum of the vortex rings is thought to correspond to the forward momentum gained by the fish. The momentum is calculated from the size and the circulation of the vortex rings. Applying this method to mullet, we derived a thrust power of 0.6 mW, a vortex power of 0.02 mW and a hydrodynamic efficiency of 97 %.

An example of the kinematic approach is Lighthill's (1970) bulk momentum theory. It uses the movements of the tail to estimate the fish-induced water movements and their energetic consequences for the fish. The parameters that enter the bulk momentum model are the angle of the tail fin with respect to the path of motion, the velocity of the tail both parallel and perpendicular to the tail blade, and the size of the tail blade. Calculation of the thrust and the waste power from the kinematics of the mullet for the same sequence (Table 4) gave less than half the thrust power (0.185 mW) compared with the flow-derived thrust, but gave a higher vortex power of 0.13 mW than did the flow-derived calculations and, consequently, a much lower efficiency (59 %).

Either the hydrodynamic approach overestimates thrust and underestimates vortex power or the kinematic estimate is too conservative. Both approaches contain several assumptions that might affect their precision. In the calculation of the energy from the wake momentum, we assumed circular vortices, although the ring diameter in the x' direction was different from the ring diameter in the y' direction. We also assumed a constant vorticity centred in the core of the vortex. Both assumptions are rather robust against violations. The calculation of the waste energy from the vortex is only valid if the vortex core diameter is smaller than 0.25 vortex ring diameters. In the mullet, the core diameter is between 0.19 and 0.28 ring diameters. Spedding (1986) suspected that the vortex ring approach underestimated the costs of locomotion because not all energy shed in the wake may be contained in the vortex rings.

The bulk momentum model assumes that the flows induced by the body movements cancel each other out over a complete tailbeat cycle and that only the flow shed at the tail contributes significantly to the thrust. With vortex structures lying at the heart of momentum flux and hence thrust generation in the inertial flow regime, the fish needs to invest energy into generating vortices to propel itself (Rayner, 1995). Taking this into consideration, the circulating flows generated by the undulating body might contribute significantly to the vortices shed at the tail. A rough estimate of the body contribution can

be obtained from the changes in the flow speed adjacent to the fish's body. Along the body, water is accelerated to peak speeds of 30–50 mm s^{-1} in the pressure and suction zones. In the tail region, the water is accelerated further to peak speeds of 100 mm s^{-1}. The water is accelerated along the first two-thirds of the body to almost half its final speed, while the posterior third of the body accounts for the acceleration to the flow final speed. With the body wave travelling at a constant speed along the body, the acceleration along the anterior part of the body takes place over twice the distance and thus twice the time as the acceleration along the posterior third of the body. This would mean that the acceleration along the anterior two-thirds of the body is half the acceleration along the posterior third of the body. Consequently, the anterior body contributes roughly a third of the total energy added to the water, with the tail region adding the remainder.

The present analysis of a two-dimensional view of the wake behind a swimming mullet is consistent with the three-dimensional chain of vortex rings postulated on theoretical grounds (Lighthill, 1975; Videler, 1993) and observed for several fish species (Rosen, 1959; Aleyev, 1977; Blickhan *et al.* 1992). The tail sheds two start–stop vortices per tailbeat cycle, forming a wake of alternating vortices in the medio-frontal plane of the fish. The power values derived from the wake using the vortex ring model (Spedding *et al.* 1984) yield thrust values of less than 1 mW with a hydrodynamic efficiency greater than 90 %. Expressing the thrust energy as the costs of moving the fish's body mass one body length yields 0.02 J N^{-1} m^{-1}. This external cost of transport for a mullet swimming steadily at a speed close to its maximum range speed (Tucker, 1970) is an order of magnitude smaller than the total cost of transport for undulatory swimmers at optimal swimming speed (Videler, 1993).

List of symbols

A_b	amplitude of the body wave
A_s	amplitude of the propulsive wave
A_{tail}	amplitude of the body wave at the tail
B	a constant depending on the vorticity profile of a vortex, equivalent to $\bar{A}$ of Spedding *et al.* (1984) and A of Lamb (1932)
d	discriminant for complex eigenvalues
E_T	thrust energy
E_L	self-energy of the vortex ring
f	tailbeat frequency
F	feathering parameter
I	momentum of the vortex ring
L	body length of the fish
l_x	distance between consecutive vortices in the x direction
l_y	distance between consecutive vortices in the y direction
p	phase of the body wave
P_L	vortex power
P_T	thrust power
R	radius of the vortex ring
R_0	radius of the vortex core
St	Strouhal number
T	duration of the tailbeat cycle
U	swimming speed of the fish
u	flow velocity component parallel to the x'-axis
V	speed of the propulsive wave parallel to the y'-axis
v	flow velocity component
x	mean path of motion of the fish
y	direction of the lateral displacement of the tail
α	momentum angle of the jet flow
β	maximum angle between the tail blade and the path of motion
Γ	circulation of the vortex
η	efficiency
φ	momentum angle of the vortex ring
λ_b	body wavelength
λ_s	propulsive wavelength (stride length)
θ	divergence
ρ_w	density of water (=1021 kg m^3)
ω	vorticity

We would like to thank the Sea Life Centre in Scheveningen for the mullet and BASF for providing the polystyrene particles. U.K.M. would like to thank Thomas Weber for comments on the manuscript and R. Blickhan for inspiring many of the ideas presented here on fish hydrodynamics. The manuscript was greatly improved by the kind comments of two anonymous referees.

References

AHLBORN, B., HARPER, D. G., BLAKE, R. W., AHLBORN, D. AND CAM, M. (1991). Fish without footprints. *J. theor. Biol.* **148**, 521–533.

ALEYEV, Y. G. (1977). *Nekton*. The Hague: Dr W. Junk. 435pp.

BLICKHAN, R., KRICK, C., ZEHREN, D. AND NACHTIGALL, W. (1992). Generation of a vortex chain in the wake of a subundulatory swimmer. *Naturwissenschaften* **79**, 220–221.

CHEN, C. J., KIM, Y. G. AND WALTER, J. A. (1993). Progress in quantitative flow visualisation and imaging process. In *Atlas of Visualisation*, pp. 279–296. Oxford: Pergamon Press.

GRAY, J. (1933). Studies in animal locomotion. I. The movement of fish with special reference to the eel. *J. exp. Biol.* **10**, 88–104.

GRAY, J. (1968). *Animal Locomotion*. London: Weidenfeld and Nicholsen.

HERTEL, H. (1966). *Structure, Form, Movement*. New York: Reinhold Publishing Corp. 251pp.

HESS, F. AND VIDELER, J. J. (1984). Fast continuous swimming of saithe (*Pollachius virens*): a dynamic analysis of bending moments and muscle power. *J. exp. Biol.* **109**, 229–251.

HINSCH, K. D. (1993). Particle image velocimetry. In *Speckle Metrology* (ed. R. S. Sirohi), pp. 235–324. New York: Marcel Dekker Inc.

KEANE, R. D. AND ADRIAN, R. J. (1991). Optimization of particle image velocimeters with multiple-pulsed systems. Paper 12.4. In *Proceedings of the Fifth International Symposium on Application*

of Laser Techniques to Fluid Mechanics, Lisbon, Portugal. Lisbon: Ladoan Instituto Superior Tecnico.

LAMB, H. (1932). *Hydrodynamics*. 6th edition. Cambridge: Cambridge University Press. 738pp.

LIGHTHILL, M. J. (1969). Hydromechanics of aquatic animal locomotion. *A. Rev. Fluid Mech.* **1**, 413–446.

LIGHTHILL, M. J. (1970). Aquatic propulsion of high hydrodynamic efficiency. *J. Fluid Mech.* **44**, 265–301.

MAXWORTHY, T. (1977). Some experimental studies of vortex rings. *J. Fluid Mech.* **81**, 465–495.

MCCUTCHEN, C. W. (1977). Froude propulsive efficiency of a small fish, measured by wake visualisation. In *Scale Effects in Animal Locomotion* (ed. T. J. Pedley), pp. 339–363. London: Academic Press.

MERZKIRCH, W. (1974). *Flow Visualisation*. New York: Academic Press.

RAYNER, J. M. V. (1979). A vortex theory of animal flight mechanics. *J. Fluid Mech.* **91**, 731–763.

RAYNER, J. M. V. (1995). Vortex wakes of vertebrates. In *Biological Fluid Dynamics* (ed. C. P. Ellington and T. J. Pedley), pp. 131–155. Cambridge: The Company of Biologist Ltd.

ROSEN, M. W. (1959). *Water Flow About a Swimming Fish*. China Lake, CA: US Naval Ordnance Test Station TP 2298. 96pp.

SPEDDING, G. R. (1986). The wake of a jackdaw (*Corvus monedula*) in slow flight. *J. exp. Biol.* **125**, 287–307.

SPEDDING, G. R. (1987). The wake of a kestrel (*Falco tinnunculus*) in flapping flight. *J. exp. Biol.* **127**, 59–78.

SPEDDING, G. R., RAYNER, J. M. V. AND PENNYCUICK, C. J. (1984). Momentum and energy in the wake of a pigeon (*Columbia livia*) in slow flight. *J. exp. Biol*. **111**, 81–102.

STAMHUIS, E. J. AND VIDELER, J. J. (1995). Quantitative flow analysis around aquatic animals using laser sheet particle image velocimetry. *J. exp. Biol.* **198**, 283–294.

TRIANTAFYLLOU, M. S., TRIANTAFYLLOU, G. S. AND GOPALKRISHNAN, R. (1991). Wake mechanics for thrust generation in oscillating foils. *Phys. Fluids* A **3**, 2835–2837.

TRIANTAFYLLOU, M. S., TRIANTAFYLLOU, G. S. AND GROSENBAUGH, M. A. (1993). Optimal thrust development in oscillating foils with application to fish propulsion. *J. Fluid & Structures* **7**, 205–224.

TUCKER, V. A. (1970). Energetic cost of locomotion in animals. *Comp. Biochem. Physiol.* **34**, 841–846.

VIDELER, J. J. (1993). *Fish Swimming*. London: Chapman & Hall. 260pp.

VIDELER, J. J. AND HESS, F. (1984). Fast continuous swimming of two pelagic predators, saithe (*Pollachius virens*) and mackerel (*Scomber scombrus*): a kinematic analysis. *J. exp. Biol.* **109**, 209–228.

WARDLE, C. S., VIDELER, J. J. AND ALTRINGHAM, J. D. (1995). Tuning in to fish swimming waves: body form, swimming mode and muscle function. *J. exp. Biol.* **198**, 1629–1636.